INSTITUTE OF PHYSICS PUBLISHING PLASMA PHYSICS AND CONTROLLED FUSION

Plasma Phys. Control. Fusion **44** (2002) B323–B338 PII: S0741-3335(02)52285-5

Atomic data for modelling fusion and astrophysical plasmas

H P Summers[1], N R Badnell[1], M G O'Mullane[1], A D Whiteford[1], R Bingham[2], B J Kellett[2], J Lang[2], K H Behringer[3], U Fantz[3], K-D Zastrow[4], S D Loch[5], M S Pindzola[5], D C Griffin[6] and C P Ballance[6]

[1] University of Strathclyde, 107 Rottenrow, Glasgow G4 0NG, UK
[2] Rutherford Appleton Laboratory, Chilton, Didcot OX11 0QX, UK
[3] University of Augsburg, D-86159 Augsburg, Germany
[4] Euratom/UKAEA Fusion Association, Culham Science Centre, Abingdon, Oxon OX14 3EA, UK
[5] Auburn University, Auburn, Alabama, AL 36849, USA
[6] Rollins College, Winter Park, Florida, FL 32789, USA

Received 13 August 2002
Published 21 November 2002
Online at stacks.iop.org/PPCF/44/B323

Abstract

Trends and focii of interest in atomic modelling and data are identified in connection with recent observations and experiments in fusion and astrophysics. In the fusion domain, spectral observations are included of core, beam penetrated and divertor plasma. The helium beam experiments at JET and the studies with very heavy species at ASDEX and JET are noted. In the astrophysics domain, illustrations are given from the SOHO and CHANDRA spacecraft which span from the solar upper atmosphere, through soft x-rays from comets to supernovae remnants. It is shown that non-Maxwellian, dynamic and possibly optically thick regimes must be considered.

The generalized collisional-radiative model properly describes the collisional regime of most astrophysical and laboratory fusion plasmas and yields self-consistent derived data for spectral emission, power balance and ionization state studies. The tuning of this method to routine analysis of the spectral observations is described. A forward look is taken as to how such atomic modelling, and the atomic data which underpin it, ought to evolve to deal with the extended conditions and novel environments of the illustrations. It is noted that atomic physics influences most aspects of fusion and astrophysical plasma behaviour but the effectiveness of analysis depends on the quality of the bi-directional pathway from fundamental data production through atomic/plasma model development to the confrontation with experiment. The principal atomic data capability at JET, and other fusion and astrophysical laboratories, is supplied via the Atomic Data and Analysis Structure (ADAS) Project. The close ties between the various experiments and ADAS have helped in this path of communication.

1. Introduction

To a large extent the ways atomic data are used in the gross interpretation of laboratory fusion and astrophysical plasmas are the same as they were twenty-five years ago. Also, the precursors of many of the methods for atomic rate calculation—multi-electron multi-configuration structure, distorted wave cross-sections, close coupling and incipient *R*-matrix techniques—were in place at that time. By the present day then we might have expected to have everything we need.

In reality, though, it is not as simple as that. Both in fusion and astrophysics, new approaches to spectroscopic measurement of enhanced diagnostic impact are continually being recognized for which it is found that earlier systematic large-scale production of atomic data is inadequate. Perhaps the original range and working precision were inappropriate and the atomic physics work must be extended with more powerful techniques and with clearer focus. Some such changes have occurred since last reviews of this kind by the authors about four years ago (Summers *et al* 1998). In particular, what might be called 'special feature' analysis is growing, non-Maxwellian environments definitely warrant attention and heavy species—which previously have been avoided—can no longer be so avoided. Finally, we clearly recognize that, in the confrontation with experimental measurement, error analysis is mandatory. Yet atomic physics inputs to this confrontation are largely from theoretical sources with no 'error' attached. This position is untenable.

In this review, we shall briefly examine some observations and use these to establish the main types of atomic data input required. This is not new, but the required scope and the parametric dependences appropriate to shared astrophysical and fusion application are usefully restated. Then we focus on the newer issues of the previous paragraph, and seek to draw out what is required and what is being done about them. These sections should not be misinterpreted as completed and existing work, but rather as an attempt to spell out how they might be achieved. The paper is not a catalogue of atomic data or even methods. There are many atomic databases in the world, readily accessible on the world wide web, where such lists can be found.

Some of the methods described here have been implemented in the Atomic DATA and Analysis Structure (ADAS) Project (Summers, 1993, 2001). Illustrations are mostly drawn from ADAS codes and databases, from the Joint European Torus (JET) fusion experiment and from the Solar and Heliospheric Observatory (SOHO) and the CHANDRA X-ray Observatory astrophysical spacecraft.

2. Some observations

Figure 1 is a portion of the normal incidence survey spectrum of the quiet sun from the CDS spectrometer on the SOHO spacecraft. The whole normal incidence spectrum spans from 308 to 381 Å and 513 to 633 Å (Brooks *et al* 1999). In the region 340–365 Å, the spectrum is dominated by iron ions, at 368 Å, we see the strong Mg IX multiplet and at 584 Å, the He I resonance line. Moving into the portion of spectrum shown in figure 1, at 591.4 Å, we see a very weak line, the He I intercombination, which is the sole indicator in the EUV range of the strong triplet side emission from He I in the visible. Finally from 595 to 630 Å, we see several strong multiplets of intermediate ionization stages of the light elements, especially oxygen. These spectral emissions from the solar upper atmosphere are from an electron impact excited plasma. The iron line emissions from the corona are formed in a plasma of electron temperature $T_e \sim 10^6$ K and electron density $N_e \sim 10^{10}$ cm^{-3} close to stationary ionization balance. Similar lines of argon, iron and nickel are seen in fusion plasmas, also electron excited but at electron density $N_e \sim 10^{14}$ cm^{-3} and in diffusive ionization balance. Such densities and

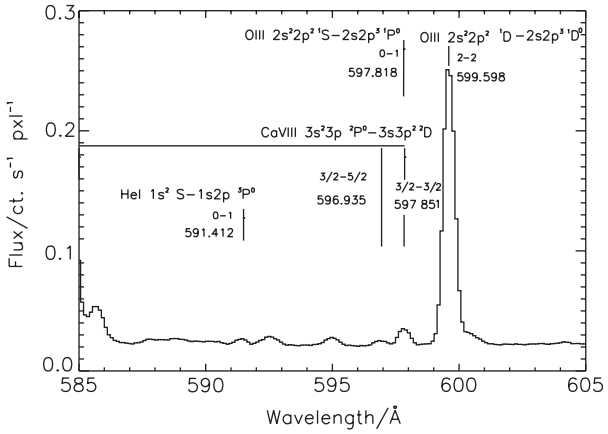

Figure 1. Portion of the analysed quiet sun spectrum from the normal incidence spectrometer, NIS-2, of the coronal diagnostic spectrometer CDS on the SOHO spacecraft (Brooks *et al* 1999). The He I intercombination line observation was a first identification in the sun. The ratio of this line to the strong He I resonance line at 584.340 Åformed in the lower chromosphere is markedly affected by optical thickness.

the transport mean that in the fusion experiment case, the effective recombination and ionization rates and emissivities must be known (and at finite electron density) for modelling and analysis whereas in the solar case, equilibrium ionization balance emission in the 'coronal' (low density) picture is more nearly sustainable (but see Lanzafame *et al* 2002). The He I spectrum is being emitting in the low chromosphere and the resonance line is optically thick. Helium is of course the ash of the fusion reactor, but is also introduced (by gas puffs and subsonic & supersonic jets) as a diagnostic species for the plasma edge and scrape-off-layer. The He I spectrum in the latter case is electron excited, but in a highly dynamic, ionizing, but optically thin environment. Also He^0 may be injected as a neutral beam, with individual atom energies $\sim$30–40 keV amu^{-1}, although D^0 is the usual injected species in heating beams. The excitation of such beam atoms is primarily by collision with the plasma ions and, in particular, they can undergo charge exchange reactions with the various bare nuclei of impurities in the plasma. A helium neutral beam into a pure helium plasma is a situation not encountered in astrophysics and rarely in fusion and the observations (see figure 2) reveal the spectral signature of unusual, but strong reactions, such as double charge transfer. The He I resonance lines in low-pressure discharges are again optically thick and the He^0 metastables are quenched by diffusion to the walls. Modelling in this regime samples a different part of the electron collision database.

The light element ions such as the carbon ions, seen radiating in the quiet sun spectrum, are similar radiators in the divertors of fusion plasmas, albeit at higher electron densities and with strong influence of wall and recycling sources. Moving away from the divertor strike zones towards the confined plasma, we progress through higher ionization stages up to the bare nuclei. Moving upward in the solar atmosphere, we see the same progression with the bare nuclei of carbon, nitrogen, oxygen, along with protons and electrons, escaping in the solar wind and within which they are spectroscopically invisible. However, the solar wind does impinge on planetary atmospheres and on ebullient cometary atmospheres. CHANDRA soft x-ray spectral observations of comets show emission from such species (particular K-shell lines) again as shown in figure 3. The emission, though, is complex, with a bremsstrahlung contribution along with spectrum lines which appears to be non-thermal. The proposed mechanism is that the streaming solar wind plasma, encountering the weakly ionized comet atmosphere, provokes a modified two-stream instabilty which, in turn, energises the electron

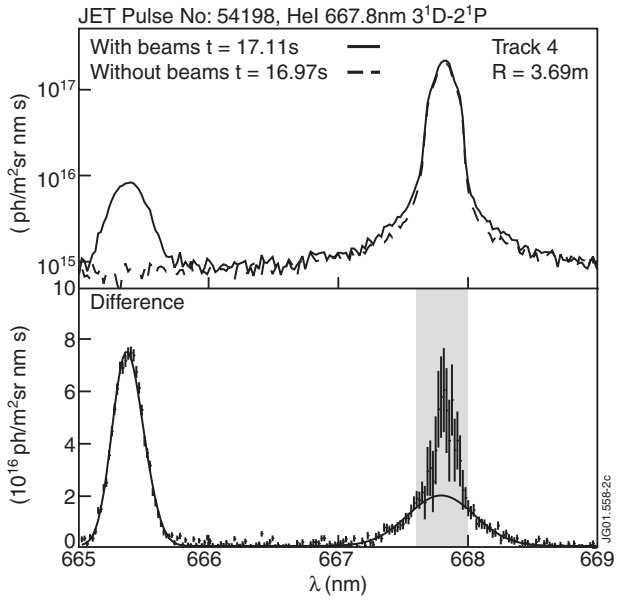

Figure 2. These JET spectra arise from fast neutral helium beam injection into a helium plasma. The neutral beams are modulated allowing distinction of beam driven and non-beam driven emission. The features at 6654 and 6678 Åare both the He I $3\,^1\mathrm{D} - 2\,^1\mathrm{P}$ line, the former being Doppler shifted beam emission in the spectrometer line-of-sight. The difference spectrum shows a hot (core plasma) component at the unshifted position. This is evidence of the double charge transfer reaction from He^0 beam atoms to He^{+2} nuclei in the plasma (Zastrow *et al* 2002). The excitation of beam atoms in the plasma is primarily due to ion impact and not electron impact. In practice, the shaded region is excluded when fitting the broad feature.

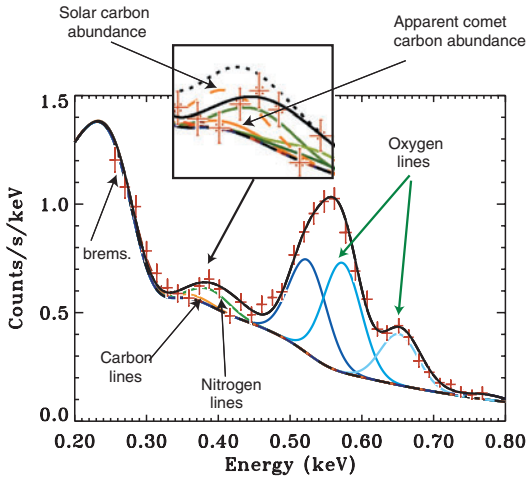

Figure 3. Soft x-ray spectrum of the comet LINEAR 1999 S4 is shown observed by the ACIS-S instrument on the CHANDRA spacecraft (Lisse *et al* 2001). The spectrum is composed of lines and a bremsstrahlung continuum which appears non-thermal. Spectral fitting using theoretical emission functions shows the spectral decomposition and allows deduction of relative light element abundances. The experimental data are the crosses. The solid curve is the theoretical spectrum with adjusted abundances. In the inset, the dotted line shows the theoretical spectrum assuming the solar carbon abundance. It is noted that LINEAR 1999 S4 is underabundant in carbon and this is clearly indicated by the model fit (Kellett *et al* 2002).

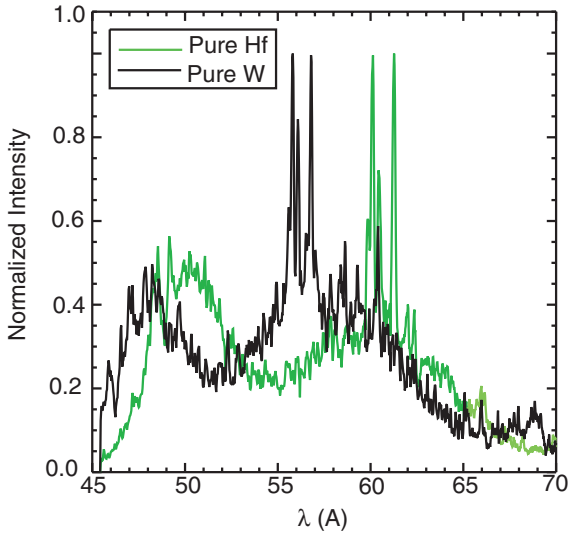

Figure 4. The XUV spectra are of Hf and W separately ablated by laser into the JET plasma. These complex spectral features are largely unresolved, but the envelopes are distinctive and characteristic. Even nearby elements such as these second long period neighbours are clearly distinguishable. Using the individual experimental signatures, the spectrum of a mixed Hf/W target ablation was successfully resolved into the proportions of Hf and W penetrating into the core plasma.

distribution. Such a phenomenon is probably quite widely occurring in astrophysics (planetary atmospheres, supernovae remnants, etc) but in different energy regimes. Non-thermal electron distributions but with depleted high-energy tails (Druyvesteyn distributions) occur in low-pressure discharges and non-thermal distributions with both enhanced and reduced high-energy Maxwellian tails are certainly expected in various parts of the fusion plasma.

In high-temperature plasmas such as flares and core fusion plasma as well as in cosmic sources, we note that species such as argon, calcium, iron and nickel show well-known and distinctive features in the soft x-ray—the so-called 'satellite line' spectra. Analysis considers the set of lines collectively and their differential dependence on electron temperature, electron density, transient ionization state, ion temperature and impulsive flow velocity. This is the prototype for 'special features' which we return to later.

The advance towards a working fusion reactor and the appraisal of plasma facing materials for it means that the avoidance of heavy species in the past, because of their deleterious radiating efficiency in the plasma core, has had to be re-appraised. Experiments with thermally resistant materials such as tungsten do indicate encouragingly low penetration into the core plasma. Heavy species in the first and second long periods will not be fully ionized even in ITER core plasmas and so are suitable as markers, detectable spectroscopically. The survey spectrum of a heavy species such as hafnium, ablated into a fusion plasma (figure 4) in the VUV and XUV is a complex envelope of transition arrays in which the individual lines are largely unresolved. Atomic data and modelling for such species are certainly now necessary, yet the complexity does mean that somewhat different approaches from that used for light elements are required.

3. Basic collisional-radiative modelling

Four classes of derived atomic coefficients provide the basic need for both spectral analysis and modelling of spectral emission in thermal astrophysical plasmas and fusion plasmas. These

are the collisional-radiative coefficients, photon emissivity coefficients, reciprocal photon efficiencies and contribution functions. They arise from the recognition that in a plasma there are large populations (ground states of ions) which evolve slowly and therefore can be in spatial or temporal non-equilibrium. These populations must be obtained in specific models of actual plasmas which include sources, geometry and transport parameters. The atomic collisional-radiative coefficients are the enabling coefficients for such modelling, namely the source terms, but do not provide the solution. The principal coefficients are the effective recombination and ionization coefficients and the radiative power loss coefficients. By contrast, the photon emissivity coefficients depend on local conditions only and allow actual emission to be reconstructed once the dominant populations have been determined. The photon efficiencies are idealizations, used mostly in fusion, to infer particle influxes from spectral line intensities. The contribution functions are also idealizations, used mostly in astrophysics, which bypass the specific transport modelling by assuming dominant populations are in local stationary ionization balance.

To cope with all reasonable ranges of dynamic thermal plasma in low- to medium-density plasma excluding short-period observations of the most highly impulsive events, the group of dominant populations is expanded to include low lying metastable states of ions and the collisional-radiative coefficients are renamed the generalized collisional-radiative coefficients. All these coefficients depend on both local electron temperature and electron density, although, depending on the particular coefficient, the low-density limit can be fairly closely approached at densities typical of the solar corona.

In summary, consider ions X^{+z} of the element X. The adjacent higher ionization stage is X^{+z+1}. Let the levels of the ion X^{+z} be separated into the metastable levels X^{+z}_{ρ}, indexed by Greek indices, and excited levels X^{+z}_{i}, indexed by Roman indices. The collective name, metastable states, as used here includes the ground state. The 'initiating' driving mechanisms considered for populating the excited levels X^{+z}_{i} are excitation from the metastable levels X^{+z}_{ρ} and recombination from the metastable levels of the adjacent ion X^{+z+1}_{ν}. Collisional and radiative processes between all levels then redistribute populations. The dominant population densities of the ions in the plasma are those of the levels X^{+z}_{ρ} and X^{+z+1}_{ν} denoted by N_{ρ} and N^{+}_{ν}, respectively. They, or at least their ratios to N_1, are assumed known from a dynamical ionization balance. The excited populations, denoted by N_i, are assumed to be in a quasi-static equilibrium with respect to the dominant populations:

$$N_j \equiv \sum_{\sigma=1}^{M_z} F^{(\mathrm{exc})}_{j\sigma} N_{\mathrm{e}} N_{\sigma} + \sum_{\nu=1}^{M_{z+1}} F^{(\mathrm{rec})}_{j\nu} N_{\mathrm{e}} N^{+}_{\nu}. \tag{1}$$

The $F^{(\mathrm{exc})}_{j\sigma}$ and $F^{(\mathrm{rec})}_{j\nu}$ are the effective contributions to the excited populations from excitation from the metastables and from free electron capture by parent metastables. All these coefficients depend on density as well as temperature. The actual population density of an ordinary level may be obtained from them when the dominant population densities are known. The population equation solution also gives the generalized collisional radiative coefficients ($\mathcal{GCR}$s), which are the first of our essential coefficients. These are the ionization coefficients $S_{\mathrm{CD},\sigma\to\nu}$ and the free electron recombination coefficients $\alpha_{\mathrm{CD},\nu\to\rho}$. The subscript 'CD' indicates that the collisional-radiative model includes dielectronic recombination. The radiated power loss coefficients separated into parts driven from X^{+z}_{ρ} and X^{+z+1}_{ν}, respectively, that is the total low-level line power (LT) $P_{\mathrm{LT},\sigma} = \sum_{k,j} \Delta_{kj} A_{j\to k} F^{(\mathrm{exc})}_{j\sigma}$ and the bremsstrahlung, recombination and cascade power (RB) $P_{\mathrm{RB},\nu} = \sum_{k,j} \Delta_{kj} A_{j\to k} F^{(\mathrm{rec})}_{j\nu} + P_{\mathrm{FB},\nu} + P_{\mathrm{FF},\nu}$. They are obtained by summing over the population structure, and integrating over the free bound (FB) and free–free (FF) contributions. The derived coefficients associated with individual

spectrum line emission are the photon emissivity coefficients ($\mathcal{PEC}$s). From equation (1), the emissivity in the spectrum line $j \rightarrow k$ is

$$\epsilon_{j\rightarrow k} = A_{j\rightarrow k}\left(\sum_{\sigma=1}^{M_z} F_{j\sigma}^{(\mathrm{exc})} N_\mathrm{e} N_\sigma + \sum_{\nu=1}^{M_{z+1}} F_{j\nu}^{(\mathrm{rec})} N_\mathrm{e} N_\nu\right). \tag{2}$$

This allows specification of the excitation photon emissivity coefficient

$$\mathcal{PEC}_{\sigma,j\rightarrow k}^{(\mathrm{exc})} = A_{j\rightarrow k} F_{j\sigma}^{(\mathrm{exc})} \tag{3}$$

and the recombination photon emissivity coefficient

$$\mathcal{PEC}_{\nu,j\rightarrow k}^{(\mathrm{rec})} = A_{j\rightarrow k} F_{j\nu}^{(rec)}. \tag{4}$$

Each of these coefficients is associated with a particular metastable σ or ν of the X^{+z} or X^{+z+1} ions, respectively. Excitation and recombination photon emissivity coefficients are illustrated in figure 5. The photon efficiency, which is really meaningful only for the excitation driven part, is simply the $\mathcal{PEC}_{\sigma,j\rightarrow k}^{(\mathrm{exc})}$ divided by the $S_{\mathrm{CD},\sigma}$.

The equilibrium fractional abundances of the dominant populations $N_\rho^{(z)}/N_\mathrm{tot}$, where $N_\mathrm{tot} = \sum_{z=0}^{z_0}\sum_{\rho=1}^{M_z} N_\rho^{(z)}$, are determined by the stationary balance of the ionization and recombination rates using the effective rates $S_{\mathrm{CD},\sigma\rightarrow\nu}$ and $\alpha_{\mathrm{CD},\nu\rightarrow\rho}$, together with some additional cross-coupling coefficients in the metastable case. The contribution function, called the $\mathcal{GTN}$, the last of the key coefficients, is then defined as

$$\mathcal{GTN}_{j\rightarrow k}^{(z)} = \frac{\sum_{\sigma=1}^{M_z} \mathcal{PEC}_{\sigma,j\rightarrow k}^{(\mathrm{exc})} N_\sigma^{(z)}}{N_\mathrm{tot}} + \frac{\sum_{\nu=1}^{M_{z+1}} \mathcal{PEC}_{\nu,j\rightarrow k}^{(\mathrm{rec})} N_\nu^{(z+1)}}{N_\mathrm{tot}}. \tag{5}$$

These expressions are simpler when only ground states are considered and if the recombination part is neglected. This is the usual procedure for the $\mathcal{GTN}$ of solar astrophysics. The typical behaviour of $\mathcal{GTN}$s as a function of electron temperature is shown in figure 6.

From the atomic physics and atomic data point of view, each of these coefficients represents the resultant effect of possibly many individual reactions, depending on the electron temperature and electron density and the particular coefficient. They are computed by calculation of the populations of all the excited levels of each ion in a quasi-static balance with the dominant populations. Their automatic calculation for all conditions of interest means that complete assemblies of fundamental individual reaction data of adequate precision must be available for every ion of interest. Such general availability is true at levels of precision around a factor $\sim$2 or 3 but not at the level of $\sim$20% which is the aspiration of high-quality spectral analysis. $\mathcal{GCR}$ modelling is almost complete for light elements up to neon, with substantial high-quality fundamental cross-section data (R-matrix, extended energy range, $\Delta n_\mathrm{g} \geqslant 1$ where Δn_g denotes number of n-shells above the ground). For heavier elements, fundamental data is selective and incomplete at this level. The products of the Iron Project (mostly $\Delta n_\mathrm{g} = 0$) (Hummer *et al* 1993) and the associated RmaX Project (few electron iso-electronic sequences so far) (Ballance *et al* 2001) is of note. The large-scale production of dielectronic data and ionization data in intermediate coupling for heavier species is internationally organized and progresses.

4. The analysis of error in forward modelled theoretical coefficients

It has been usual to use the derived atomic coefficients of the sort defined above as given, i.e. as though they were exact. In very large part the underlying fundamental reaction cross-sections and Maxwell averaged rate coefficients come from theory. Assignment of an error to theory is uncommon, although there are usually somewhat vague opinions as to the broad likely

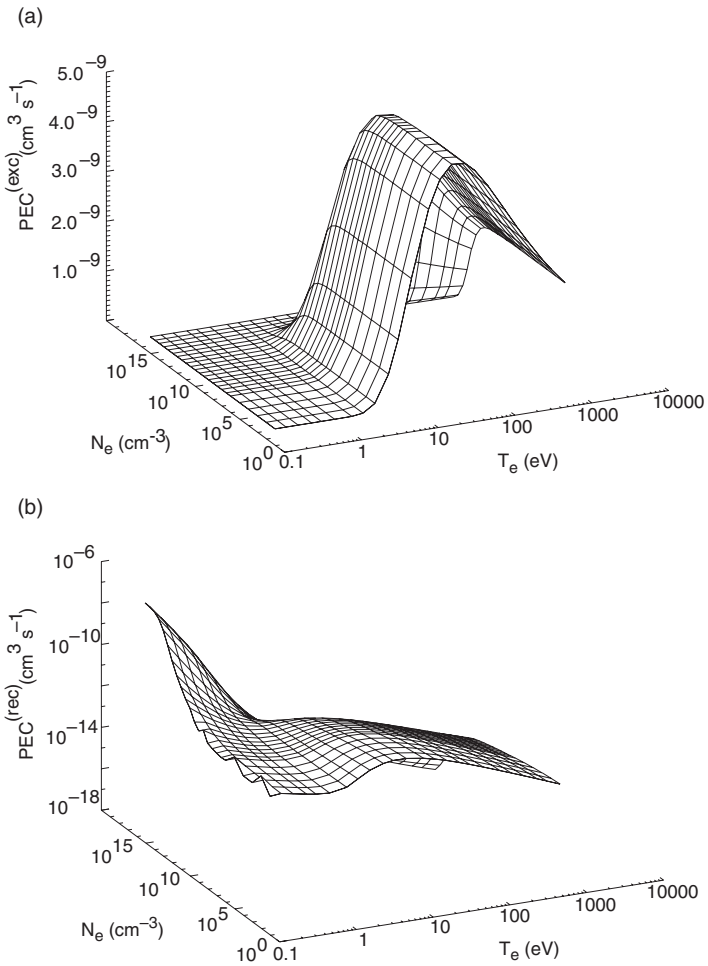

Figure 5. Excitation and recombination photon emissivity functions, $\mathcal{PEC}$s, driven by the ground metastables, are shown for the C II 858 Åspectrum line. The coefficients depend on both electron temperature and electron density. The (exc) part decreases at high electron density due principally to stepwise ionization losses from the upper level of the transition. The behaviour of the (rec) part shows both suppression of dielectronic recombination at moderate density and then enhancement due to three-body recombination at high density and low temperature.

uncertainty of a particular approximation. In practice, one finds that the nominal precision of a method is rarely met and the word of mouth statements are over optimistic. Clearly, assignment of uncertainties to theoretical cross-section data is difficult. Nonetheless it does matter, otherwise inferences drawn from the comparison with experiment may be misleading. The effective coefficients, of course, depend on many individual reactions, some well known and others less well known, and the balance of importance of the individual contributors depends on the electron temperature and density. We start from the premise that there are errors assigned to each individual fundamental reaction rates which are Gaussian distributed and independent. Two pieces of information are valuable. For the theoretical atomic physicist, it is helpful to know the individual reaction which is the dominant source of error in the derived coefficient as a motivation for refinement of theoretical calculations. For the spectral analyst, the cumulative statistical error on the derived coefficient is what matters. Both errors

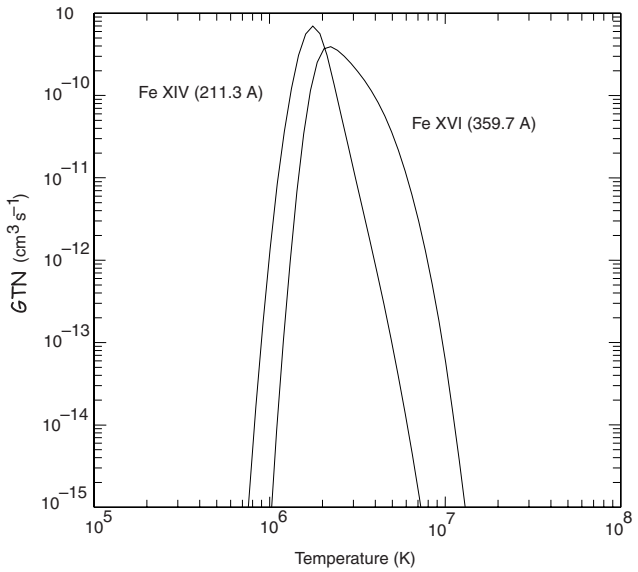

Figure 6. $\mathcal{GTN}$s for some iron spectrum lines at constant electron pressure $10^{14}\,\mathrm{cm}^{-3}\,\mathrm{K}$. The functions, which incorporate the equilibrium ionization balance, are strongly peaked in electron temperature and so are suited to diagnostic techniques such as differential emission measure analysis. Theoretical functions including dependence on both temperature and density allow the double-differential approach. The functions shown here include the $N_\mathrm{e}/N_\mathrm{H}$ relative abundance factor as a function of temperature in the solar atmosphere, as is normal in solar astrophysical usage.

can be estimated, the first by varying each fundamental reaction rate by its error in turn and recalculating the derived coefficient and the latter by Monte Carlo sampling from all the individual errors and the repeating the calculation of the derived coefficient and the process many times until statistics are built up. Figure 7 shows the upper error surface on the excitation $\mathcal{PEC}$ for a He I spectrum line.

It is our opinion that a systematic approach to error is overdue in this area. We distinguish 'locked' parameters as distinct from 'search' parameters in optimized fitting of models to experiment. Search parameters return a fit uncertainty or confidence level, the locked parameters must carry an error with them. An effective rate coefficient is such a locked parameter. Its Gaussian error is computed from the errors of the fundamental reaction rates as above. In an organized framework, the $\mathcal{PEC}$ database of (.dat files) have an error database (.err files) exactly paralleling it in archive library structure and in file organization. The issue then is realistic errors in the fundamental reactions. It must be accepted that for many transitions, particularly those amongst highly excited states, a general and imprecise error is all that can be achieved. However, the focus of attention in calculation of electron impact cross-sections for the upper levels of spectrosopically observed lines is on using high-quality methods such as *R*-matrix. The expert calculator assesses convergence of results by varying the number of spectroscopic levels included, varying pseudo-state basis sets, switching on and off resonance contributions, checking the difference between resonance contributions in term (LS) and intermediate (IC) coupling and by checking 'top-up' and the approach to the high-energy limit points. These procedures do yield an estimate of error. This does not detect systematic error but does provide a starting point for the organized error analysis of derived coefficients with which we are concerned here. There is no systematic availability of (.err data) for derived coefficients at this stage in time.

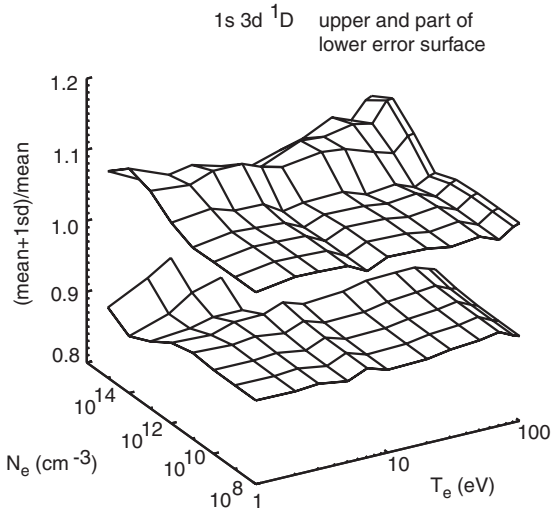

Figure 7. Upper and lower standard error surfaces for the part of the He^{+0} 1s3d ^{1}D population driven by excitation. A portion of the lower surface has been deleted for clarity. These cumulative errors are from statistical sampling of the errors in the fundamental rate coefficients. The population error is close to that for the excitation-driven emissivities from that upper level.

5. Complex atom modelling and envelope features

As indicated in the introduction, we would like to continue our spectral analysis and modelling capability onwards and upwards to heavier elements, with more ions each with more electrons. Partially ionized ions of elements such as silver and palladium in the first long period and tungsten and tantalum in the second long period, however, have two problems, an atomic structure which increasingly should be described in intermediate coupling and a consequent dispersion of their emitted spectrum lines into very many separated levels from many transition arrays often associated with partially filled inner shells. The spectral emission may appear grass-like or as a quasi-continuum. This may be some problem to the high-performance massively parallel computer, but even more so is it a problem for the 'hands-on' spectral analyst. There are, therefore, two problems here—coping with the magnitude of the problem and condensing it in a manner which is practicable for use. First of all, for the quasi-continuum, rather than individual lines we can treat spectral intervals. Such spectral intervals can be those corresponding to particular spectrometers. Introduce a new derived coefficient for each ion, the $\mathcal{FPEC}$ which is a function of digitized wavelength (pixel), electron temperature and electron density and is the composite of all the individual line $\mathcal{PEC}$s (subject to some broadening) which contribute to the spectral interval. In practice, the complex atom spectrum is partly some strong resolved lines and an unresolved or partially resolved envelope. The leading strong lines are identified as $\mathcal{PEC}$s in the usual manner and the rest as the $\mathcal{FPEC}$. The calculation of these $\mathcal{PEC}$s and $\mathcal{FPEC}$s requires an excited population structure calculation which is massive. However, it can be reduced and regulated by conducting parts (which give transition arrays outside the spectral region of interest) as configuration average and only those in the region of interest in full intermediate coupling J-resolution. Thus the ions of a heavy element are represented by a combination of $\mathcal{PEC}$s and $\mathcal{FPEC}$s. Figure 8 shows such an $\mathcal{FPEC}$ for the Hf^{+28} ion.

Formally, then consider a spectral interval, $[\lambda_0, \lambda_1]$, subdivided into $N_{\rm pix}$ intervals indexed by i. Also suppose that the $j \rightarrow k$ spectrum line has a normalized emission profile $\phi_{j\rightarrow k}(\lambda)$. In general, such a profile is a convolution of Doppler and instrumental functions. Then the

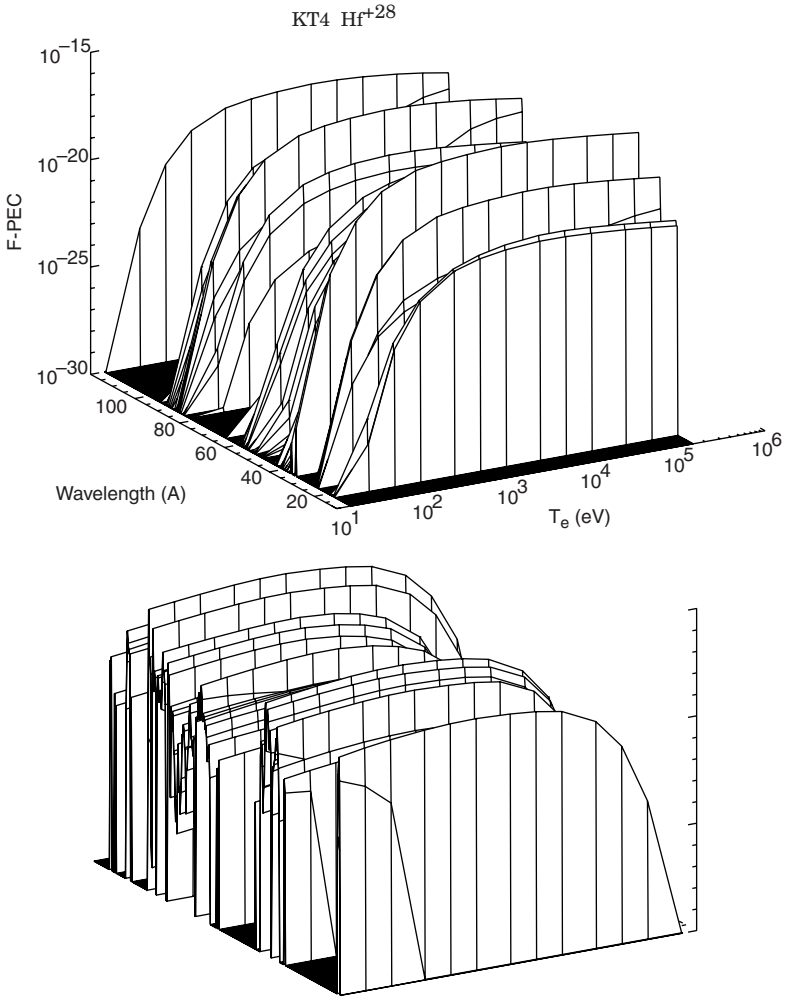

Figure 8. $\mathcal{FPEC}$ for Hf^{+28} in a segment of the XUV spectral range of the survey spectrometer (KT4) at JET. The graph is for the single electron density $N_e = 10^{14}$ cm^{-3}. The thermal broadening causes the overlapping of individual lines especially at higher temperatures, as seen in the second part of the figure, which is the view from the high-temperature side.

envelope feature photon emissivity coefficient vector is defined as

$$\mathcal{FPEC}^{(\mathrm{exc})[0,1]}_{\sigma,i} = \sum_{j,k;\lambda_{j\to k}\epsilon[0,1]} \mathcal{PEC}^{(\mathrm{exc})}_{\sigma,j\to k} \int_{\lambda_i}^{\lambda_{i+1}} \phi_{j\to k}(\lambda)\,\mathrm{d}\lambda \tag{6}$$

where $\lambda_{j\to k}$ is the natural wavelength of the $j \to k$ spectrum line. The default broadening assumed is Doppler with a Maxwellian distribution for the emitting ion at temperature, T_{ion}, equal to the electron temperature, T_e, used in the collisional-radiative modelling of the $\mathcal{PEC}$s. This constitutes a minimum broadening and a basis for adding instrumental functions, power filters, etc. The most sophisticated heavy element studies so far have focused on molybdenum and tungsten (using the code package HULLAC—cf Asmussen *et al* 1998). Systematic baseline production in line with the above prescriptions has been initiated.

6. Modelling and analysis using synthesized special features

In the fitting of observed spectra for diagnostic analysis, it is generally the relative intensities of a set of connected spectrum lines which allow inference of underlying plasma parameters. From a spectral analysis point of view, connected spectrum lines which are close together in a fairly small wavelength segment are least influenced by calibration errors and so most useful. Such connected spectrum lines are properly called feature primitives, features or super-features depending upon whether the connections are via pure branching ratios, via an excited level population balance or via an ionization balance. Ionization balance in this context may include transport and/or transient influences. The generic name feature is used for all three types of connection. In spectral measurements on real plasmas, additional unconnected spectrum lines, called ordinary lines, from different ions or elements may lie in the observed spectral segment possibly overlaying the connected group. Special spectral feature fitting distinguishes the ordinary lines + background and a special feature. It conducts a non-linear search for the parameters of both simultaneously. The observed data are fitted to the $I_k = I_k^{\mathrm{O}} + I_k^{\mathrm{F}}$ where I_k is the observed count rate at a particular detector pixel position x_k and I_k^{O} and I_k^{F} represent the ordinary line + background and the special feature parts, respectively. The ordinary lines and background are represented as several, usually simple Gaussian shaped, lines together with a constant, linear or quadratic background. That is

$$I_k^{\mathrm{O}} = b_0 + b_1 x_k + b_2 x_k^2 + \sum_{i=1}^{L} \exp\left(\frac{x_k - xo_i}{w_i}\right)^2, \tag{7}$$

where L is the number of ordinary lines in the spectrum where the ith line has central amplitude h_i, pixel position xo_i at the centre of the line and half-width w_i.

The Zeeman/Paschen–Back special feature model, illustrated in figure 9 represents I_k^{F} as

$$I_k^{\mathrm{F}} = N_{\gamma\mathrm{LS}}^{(z)} \sum_{c} E_{\mathrm{c}}(\theta, B)\psi_{\lambda_k - \lambda_{\mathrm{c}}(B) - \Delta\lambda}(T_{\mathrm{i}}, b), \tag{8}$$

where a common spectral profile for each line of the Zeeman/Paschen–Back multiplet, indexed by c of natural wavelength, $\lambda_{\mathrm{c}}(B)$, of the form $\psi_{\lambda_k - \lambda_{\mathrm{c}}(B) - \Delta\lambda}(T_{\mathrm{i}}, b)$ has been introduced. In general T_{i} is the ion temperature and b is a second parameter of the profile shape. $\Delta\lambda$ is a further parameter which is the displacement of the centroid of the Zeeman/Paschen–Back multiplet from its exact theoretical value. E denotes the generic emissivity functional and $N_{\gamma\mathrm{LS}}^{(z)}$ the multiplet population. The fit procedure is usually operated with the geometrically locked angle to the field θ and returns the magnetic flux density B and ion temperature T_{i} along with usual ordinary line Gaussian parameters.

Molecular band structures and dielectronic satellite line spectral intervals are suitable special feature candidates. Figure 9 also shows a special feature implementation of the hydrogen Balmer series through the high series members into the merged continuum. The series decrement, the individual member broadening, the merging and the underlying bremsstrahlung (hydrogen and impurities in general) provides multiple and linked plasma parameter insight. From the atomic modelling point of view, each theoretical feature is generally held as a pre-calculated, multi-parameter scan, tabulation, tuned to efficient use in optimized fitting called a 'feature file'. There is substantial fundamental legacy data for satellite line studies but it is being replaced by updated methods (R-matrix—radiation damped, frame transformations, pseudo-states). Series limit studies so far are for hydrogen and helium. Some issues are still to be resolved, especially for helium series.

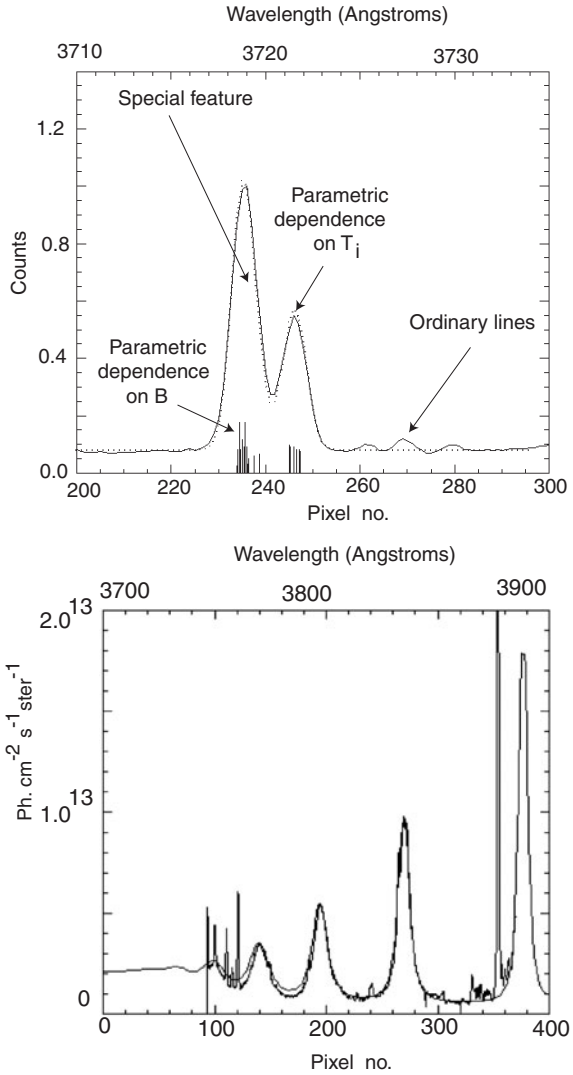

Figure 9. The top part shows a Zeeman special feature. The observed spectrum is from JET and the Zeeman split multiplet is Be III ($1s2s\,^3S$–$1s2p\,^3P$) at 3721 Å. Part of the parametric control of the special feature is indicated. Preliminary manual search in the special feature parameter space in an interactive window environment provides insight prior to automatic fitting. The bottom part shows the deuterium Balmer series limit special feature. The observed spectrum is of the JET divertor plasma in a density limit discharge. The final detail of the fit in the line shapes is of note as is the importance of handling unconnected ordinary lines in the spectral range.

7. Non-Maxwellian modelling

In low-density plasmas, such as glow discharges and RF and microwave plasma reactors, the shape of the electron distribution is strongly influenced by energy transfer to the neutral atoms. The high-energy part of the Maxwellian is selectively depleted and the shape moves to that of the Druyvesteyn pattern although actual distributions depend on the chemical composition of the plasma, as shown in figure 10. Similar patterns might be expected in strongly radiatively cooled divertors. By contrast, wave–particle interactions and plasma instability mechanisms occurring

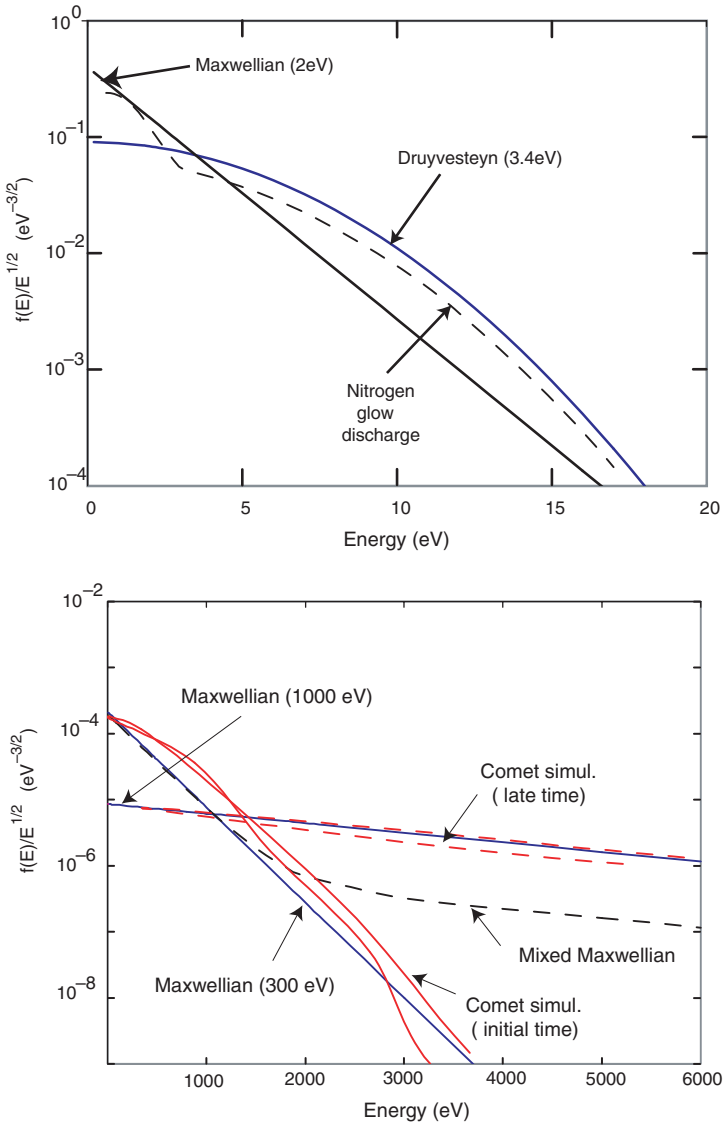

Figure 10. Top part shows electron distribution functions typical of low-temperature discharges. The Maxwell and Druvesteyn patterns are shown and a modelled case for a nitrogen plasma. The kink at ∼0.8 eV reflects the energy loss to vibrational excitation of the molecule (Behringer and Fantz 1994). The bottom part shows a higher energy environment and enhancements of the tail of the Maxwell distribution. The simulation of the energizing mechanism for the comet Hyakutake is from Dawson *et al* (1997). Note that the pick-up for electrons is almost entirely in $v_{\|}$ with respect to the magnetic field. The lack of exact symmetry between positive and negative values gives the double curves and there is some arbitrariness in the conversion to an energy distribution function for this figure.

in astrophysics and certainly also occurring in the fusion regime enhance the high-energy tail of the Maxwellian. The second illustration in figure 10 shows two time slices in a simulation of this pick-up via lower hybrid waves generated in the solar wind interaction with cometary gas. In both these situations, it is clear that we are presented with families of distributions, which can conveniently be described in terms of a single (equivalent to temperature) parameter.

It is often suggested that such distributions should simply be represented as a double Maxwellian and derived coefficients for pure Maxwellians superposed. Properly, we must return the collections of fundamental electron impact reaction data. In the ADAS project, these are generally held in a data format numbered *adf04* as Maxwell averaged collision strengths (Υs). For arbitrary electron distribution functions, we go back to the collision strengths (Ωs) themselves. These are conveniently tabulated as functions of the electron energy in threshold units (X parameter) also in the *adf04* format. We call the former *type-3* and the latter *type-1*. Explicit integration over a family of non-Maxwellian distribution functions gives a *type-4* file. Excited population modelling and derivative coefficient preparation can operate on such modified files almost transparently.

Modern calculations, especially *R*-matrix calculations, of electron impact collision cross-sections, at root, must tabulate at many thousands of energies to resolve the detailed resonance structure. Maxwell averaging smooths this structure. The new situation requires an intermediate, but explicit averaging, over intervals large compared with resonance widths, but narrow compared with relevant electron distribution functions. Such procedures can contract the *R*-matrix tabulations to well-defined *adf04 type-1* tabulations for general application and archiving. This step makes explicit the characteristic averaging widths and their appropriateness for application to arbitrary electron distribution functions—a matter which is neither clear or explicit in the many manipulations and comparisons of so-called cross-sections, which are nearly all in fact averaged cross-sections. In summary, a relatively transparent move to non-Maxwellians in the atomic modelling is possible but in terms of *adf04 type-1*. Currently there is no systematic-derived coefficient database assembled.

8. Conclusions

This paper has reviewed a number of spectroscopic observations from fusion and astrophysics, especially those which indicate that some extension of the procedures for atomic modelling of relevant derived quantities is required. For electron collision driven plasmas, new methods have been described which handle most of these requirements. Emphasis has been placed on coping with very complex atomic systems, with taking advantage of diagnostically effective special features, with the non-Maxwellian environment and with errors.

A number of forms of useful derived atomic data for application have been described. Formats for all of these data have been specified in detail in the ADAS Project. Some have achieved some general recognition in the user community and are frequently written to directly by producers of fundamental data. ADAS format *adf11* is used for the generalized collisional-radiative ($\mathcal{GCR}$) coefficients, *adf13* for reciprocal photon efficiencies ($\mathcal{SXB}$), *adf15* for photon emissivity coefficients ($\mathcal{PEC}$). *adf20* is used for the solar astrophysical contribution functions ($\mathcal{GTN}$) and *adf40* for the envelope feature emissivity coefficients ($\mathcal{FPEC}$). The specific collections of data for an ion, which allows a population structure calculation to take place, are archived in *adf04* format.

Acknowledgment

We thank the Max-Planck Institute for Plasma Physics, Garching, Germany for their kind sponsorship of a visiting position (HPS).

References

Asmussen K *et al* 1998 *Nucl. Fusion* **38** 967
Ballance C P, Badnell N R and Berrington K H 2001 *J. Phys.* B **34** 3287

Behringer K H and Fantz U 1994 *J. Phys.* D **27** 2128
Brooks D H *et al* 1999 *Astron. Astrophys.* **347** 277
Dawson J M, Bingham R and Shapiro V D 1997 *Plasma Phys. Control. Fusion.* **39** A185
Hummer D G *et al* 1993 *Astron. Astrophys.* **279** 298
Kellett B J *et al* 2002 *Astron. Astrophys.* submitted
Lanzafame A C *et al* 2002 *Astron. Astrophys.* **384** 242
Lisse C M *et al* 2001 *Science* **292** 1343
Summers H P 1993 *JET Joint Undertaking Report* JET-IR(93)07
Summers H P *et al* 1998 *Atomic and Molecular Data and their Applications* ed P J Mohr (AIP Press)
Summers H P 2001 *The ADAS User Manual, version 2.4* http://adas.phys.strath.ac.uk
Zastrow K-D *et al* 2003 *Plasma Phys. Control. Fusion* submitted